Inorg. Chem. **2003**, *42*, 4479–4484

A Layered Tungstic Acid $H_2W_2O_7 \cdot nH_2O$ with a Double-Octahedral Sheet Structure: Conversion Process from an Aurivillius Phase $Bi_2W_2O_9$ and Structural Characterization

Manabu Kudo,[†] Hajime Ohkawa,[†] Wataru Sugimoto,[‡] Nobuhiro Kumada,[§] Zheng Liu,[||] Osamu Terasaki,[⊥] and Yoshiyuki Sugahara*,[†]

Department of Applied Chemistry, School of Science and Engineering, Waseda University, Shinjuku-ku, Tokyo 169-8555, Japan, Department of Fine Materials Engineering, Faculty of Textile Science and Technology, Shinshu University, Ueda, Nagano 386-8567, Japan, Faculty of Engineering, Yamanashi University, Miyamae, Kofu, Yamanashi 400-8511, Japan, Institute of Multidisciplinary Research for Advanced Materials, Tohoku University, Aoba-ku, Sendai, Miyagi 980-8577, Japan, and Department of Physics, Graduate School of Science and CIR, Tohoku University, Aoba-ku, Sendai, Miyagi 980-8578, Japan

Received November 18, 2002

The conversion process of an Aurivillius phase, $Bi_2W_2O_9$, into a layered tungstic acid by hydrochloric acid treatment has been investigated, and resultant $H_2W_2O_7 \cdot nH_2O$ has been fully characterized. The *c* parameter of $Bi_2W_2O_9$ [2.37063(5) nm] decreases to 2.21(1) nm in an acid-treated product dried at ambient temperature. The *a* and *b* parameters of $Bi_2W_2O_9$ [$a = 0.54377(1)$ nm and $b = 0.54166(1)$ nm] also decrease slightly to $a = 0.524(1)$ nm and $b = 0.513(1)$ nm in the acid-treated product dried at ambient temperature, indicating structural changes in the ReO_3-like slabs in $Bi_2W_2O_9$ upon acid treatment. Drying at 120 °C leads to a further decrease in the *c* parameter [1.86(1) nm] with no notable change in the *a* and *b* parameters [$a = 0.5249(2)$ nm and $b = 0.513(2)$ nm]. The formation of an expandable layered structure is demonstrated by the successful intercalation of *n*-octylamine [interlayer distance 2.597(9) nm] and *n*-dodecylamine [interlayer distance 3.56(2) nm]. The compositions of the acid-treated products are determined to be $H_2W_2O_7 \cdot nH_2O$ typically with $n = 0.58$ for the air-dried product and $n = 0$ for the product dried at 120 °C. As a consequence, the composition of the layer is $H_2W_2O_7$, and the decrease in the *c* parameter upon drying is ascribable to the loss of interlayer water. Scanning electron microscopy reveals no morphological change during acid treatment, which strongly suggests a selective leaching of the bismuth oxide sheets as a reaction mechanism. High-resolution transmission electron microscopy (HREM) observation of the acid-treated product shows consistency with a structural model for $H_2W_2O_7$, derived from $Bi_2W_2O_9$ through removal of the bismuth oxide sheets and contraction along the *c* axis. HREM observation also reveals that the WO_6 octahedra arrangement changes slightly with acid treatment. A one-dimensional electron density map projected on the *c* axis for the product dried at 120 °C, $H_2W_2O_7$, shows good consistency with that calculated for the structural model.

Introduction

Several tungstic acids (alternatively referred to as tungsten trioxide hydrates) with different compositions and structures have been identified. One of these, $WO_3 \cdot 2H_2O$,[1−3] which is isostructural with $MoO_3 \cdot 2H_2O$, consists of single sheets of corner-sharing $WO_5(OH_2)$ octahedra and interlayer water.[4] $WO_3 \cdot H_2O$[1,2] can be obtained through the removal of interlayer water from $WO_3 \cdot 2H_2O$.[5] Water molecules are directly bound to tungsten atoms in $WO_3 \cdot H_2O$.[6] A colloidal tungstic acid prepared by acidification of sodium tungstate was also reported and identified as $WO_3 \cdot nH_2O$, which possesses a

* To whom correspondence should be addressed. E-mail: ys6546@waseda.jp.
[†] School of Science and Engineering, Waseda University.
[‡] Faculty of Textile Science and Technology, Shinshu University.
[§] Faculty of Engineering, Yamanashi University.
[||] Institute of Multidisciplinary Research for Advanced Materials, Tohoku University. Current address: Bio Nanotec Research Institute Inc., Sumitomofudosan-Hamacho Bldg., 3-42-3 Nihonbashi Hamacho, Chuo-ku, Tokyo 103-0007, Japan.
[⊥] Department of Physics, Tohoku University. Current address: Structural Chemistry, Arrhenius Laboratory, Stockholm University S-10691, Stockholm Sweden.

(1) Freedman, M. L. *J. Am. Chem. Soc.* **1959**, *81*, 3834−3839.
(2) Freedman, M. L.; Leber, S. *J. Less-Common Met.* **1964**, *7*, 427−432.
(3) Furusawa, K.; Hachisu, S. *Sci. Light (Tokyo)* **1966**, *15*, 115−130.
(4) Gopalakrishnan, J.; Bhuvanesh, N. S. P.; Raju, A. R. *Chem. Mater.* **1994**, *6*, 373−379.

10.1021/ic0206746 CCC: $25.00
Published on Web 06/17/2003

layered structure.[5] The hemihydrate $WO_3 \cdot 1/2H_2O$ by contrast possesses a cubic pyrochlore-type structure consisting of six-membered rings of corner-sharing WO_6 octahedra.[7−9] Water molecules are present in the tunnels consisting of WO_6 octahedra. In the structure of $WO_3 \cdot 1/3H_2O$, single-octahedral infinite sheets consisting of six-membered rings are stratified along the *c* axis with a displacement by *a*/2.[10,11] Water molecules are directly coordinated to tungsten atoms.

A variety of protonated layered oxides have been prepared from oxides through acid treatment (the so-called "*chimie douce*" approach), typically involving exchange of interlayer metal cations in the interlayer space of layered oxides with protons.[12] Ion-exchangeable layered perovskites ($M_m[A_{n-1}B_nO_{3n+1}]$; M = Rb, K, etc.; A = Sr, Ca, La, etc.; B = Ti, Nb, Ta; $m = 1$, Dion−Jacobson phases;[13,14] $m = 2$, Ruddlesden−Popper phases)[15,16] consist of interlayer cations (M) and perovskite-like slabs ($[A_{n-1}B_nO_{3n+1}]$) and can be easily converted into their protonated forms through acid treatment.[17] Aurivillius phases,[18−20] $Bi_2A_{n-1}B_nO_{3n+3}$, resulting from alternative stacking of the same type of perovskite-like slabs ($[A_{n-1}B_nO_{3n+1}]$) and bismuth oxide sheets, are known as related phases. We first reported a novel conversion of an Aurivillius phase, $Bi_2ANaNb_3O_{12}$, into a protonated form of a layered perovskite, $H_{1.8}[Sr_{0.8}Bi_{0.2}NaNb_3O_{10}]$, through selective leaching of the bismuth oxide sheets.[21−23] Subsequent reports on the conversion of other Aurivillius phases ($Bi_2CaNaNb_3O_{12}$,[23] $Bi_2SrTa_2O_9$,[24] and $Bi_2Sr_2Nb_2MnO_{12}$[17]) into corresponding protonated forms demonstrated that this route can be applied to various Aurivillius phases to prepare new protonated forms.

The preparation of tungsten-containing oxides and tungstic acids through acid treatment has also been investigated extensively. A typical example is $WO_3 \cdot 1/2H_2O$ preparation, which was achieved by acid treatment of the pyrochlore-type oxide $(A_2O)_xW_2O_6$ (A = Rb, Cs, NH_4; $0.3 < x < 0.5$).[7] Additionally, acid treatment of $LiMWO_6$ (M = Nb, Ta) resulted in the formation of $HMWO_6$ with layered structures.[25−27] Acid treatment of $LiVWO_6$[4] and $LiM'W_2O_8$[28] (M′ = Al, Fe) led, moreover, to the formation of $H_xV_xW_{1-x}O_3 \cdot yH_2O$ phases ($x = 0.125$ and 0.33), $WO_3 \cdot 2H_2O$ or $WO_3 \cdot 1/3H_2O$, but the reactions were not reported to be topotactic. Very recently, Schaak et al. have briefly reported the conversion of an Aurivillius phase, $Bi_2W_2O_9$, into $H_2W_2O_7$.[29] Since their aim was to prepare nanoscaled colloids through exfoliation, they did not establish experimental conditions for single-phase synthesis. Consequently, only XRD results were provided. In terms of the reaction mechanism, they reported that this process proceeded through selective leaching of bismuth oxide sheets.

Here, we report the conversion process of $Bi_2W_2O_9$ into single-phase $H_2W_2O_7 \cdot nH_2O$ by hydrochloric acid treatment. In the course of this study, we noted a slight contraction along the *a* and *b* axes upon acid treatment in addition to a contraction along the *c* axis, suggesting that the structure of the layers in $H_2W_2O_7 \cdot nH_2O$ is not identical to that of the ReO_3-like slabs in $Bi_2W_2O_9$. Since the structures of the perovskite-like slabs were completely retained during the conversion of the other Aurivillius phases ($Bi_2A_{n-1}B_nO_{3n+3}$; B = Nb, Ta, and Mn),[17,21−24] this observation may raise doubts about the reaction mechanism of this conversion. Thus, besides full characterization of the resulting $H_2W_2O_7 \cdot nH_2O$, we present structural considerations of $H_2W_2O_7$ (a phase obtainable by drying at 120 °C) on the basis of high-resolution transmission electron microscopy (HREM) to demonstrate that the structure of $H_2W_2O_7$ can be derived from $Bi_2W_2O_9$ through selective leaching of bismuth oxide sheets, even with a slight structural change in the ReO_3-like slab.

Experimental Section

Preparation of $Bi_2W_2O_9$. $Bi_2W_2O_9$ was prepared by calcining a stoichiometric mixture of Bi_2O_3 and WO_3 at 800 °C for 48 h with intermittent grinding, under conditions similar to those described in the previous report.[30] The phase purity was confirmed by X-ray powder diffraction (XRD) analysis. The lattice parameters were determined to be $a = 0.54377(1)$ nm, $b = 0.54166(1)$ nm, and $c = 2.37063(5)$ nm, results consistent with those of the previous report [$a = 0.5440(1)$ nm, $b = 0.5413(1)$ nm, and $c = 2.3740(5)$ nm].[31] Inductively coupled emission spectroscopy (ICP) analysis demonstrated that the Bi:W molar ratio was 1.0. These analytical results indicate the successful formation of $Bi_2W_2O_9$.

Acid Treatment of $Bi_2W_2O_9$. About 1 g of $Bi_2W_2O_9$ was added to 200 mL of 6 M HCl, and the mixture was stirred at ambient temperature for 72 h. The resultant product was a yellow powder. The same reaction was performed on a much larger scale (10 g of

(5) Chemseddine, A.; Babonneau, F.; Livage, J. *J. Non-Cryst. Solids* **1987**, *91*, 271−278.
(6) Szymański, J. T.; Roberts, A. C. *Can. Mineral.* **1984**, *22*, 681−688.
(7) Coucou, A.; Figlarz, M. *Solid State Ionics* **1988**, *28−30*, 1762−1765.
(8) Nedjar, R.; Borel, M. M.; Hervieu, M.; Raveau, B. *Mater. Res. Bull.* **1988**, *23*, 91−97.
(9) Günter, J. R.; Amberg, M.; Schmalle, H. *Mater. Res. Bull.* **1989**, *24*, 289−292.
(10) Gerand, B.; Nowogrocki, G.; Guenot, J.; Figlarz, M. *J. Solid State Chem.* **1979**, *29*, 429−434.
(11) Gerand, B.; Nowogrocki, G.; Figlarz, M. *J. Solid State Chem.* **1981**, *38*, 312−320.
(12) Gopalakrishnan, J. *Chem. Mater.* **1995**, *7*, 1265−1275.
(13) Dion, M.; Ganne, M.; Tournoux, M. *Mater. Res. Bull.* **1981**, *16*, 1429−1435.
(14) Jacobson, A. J.; Johnson, J. W.; Lewandowski, J. T. *Inorg. Chem.* **1985**, *24*, 3727−3729.
(15) Ruddlesden, S. N.; Popper, P. *Acta Crystallogr.* **1957**, *10*, 538−539.
(16) Ruddlesden, S. N.; Popper, P. *Acta Crystallogr.* **1958**, *11*, 54−55.
(17) Schaak, R. E.; Mallouk, T. E. *Chem. Mater.* **2002**, *14*, 1455−1471.
(18) Aurivillius, B. *Ark. Kemi* **1949**, *1*, 463.
(19) Aurivillius, B. *Ark. Kemi* **1949**, *1*, 499.
(20) Aurivillius, B. *Ark. Kemi* **1950**, *2*, 519.
(21) Sugimoto, W.; Shirata, M.; Sugahara, Y.; Kuroda, K. *J. Am. Chem. Soc.* **1999**, *121*, 11601−11602.
(22) Shirata, M.; Tsunoda, Y.; Sugimoto, W.; Sugahara, Y. *Mater. Res. Soc. Symp. Proc.* **2001**, *658*, GG6.24.1−5.
(23) Sugimoto, W.; Shirata, M.; Kuroda, K.; Sugahara, Y. *Chem. Mater.* **2002**, *14*, 2946−2952.
(24) Tsunoda, Y.; Shirata, M.; Sugimoto, W.; Liu, Z.; Terasaki, O.; Kuroda, K.; Sugahara, Y. *Inorg. Chem.* **2001**, *40*, 5768−5771.
(25) Kumada, N.; Horiuchi, O.; Muto, F.; Kinomura, N. *Mater. Res. Bull.* **1988**, *23*, 209−216.
(26) Bhat, V.; Gopalakrishnan, J. *Solid State Ionics* **1988**, *26*, 25−32.
(27) Bhuvanesh, N. S. P.; Gopalakrishnan, J. *Inorg. Chem.* **1995**, *34*, 3760−3764.
(28) Bhuvanesh, N. S. P.; Uma, S.; Subbanna, G. N.; Gopalakrishnan, J. *J. Mater. Chem.* **1995**, *5*, 927−930.
(29) Schaak, R. E.; Mallouk, T. E. *Chem. Commun.* **2002**, 706−707.
(30) Watanabe, A.; Goto, M. *J. Less-Common Met.* **1978**, *61*, 265−272.
(31) Champarnaud-Mesjard, J.-C.; Frit, B.; Watanabe, A. *J. Mater. Chem.* **1999**, *9*, 1319−1322.

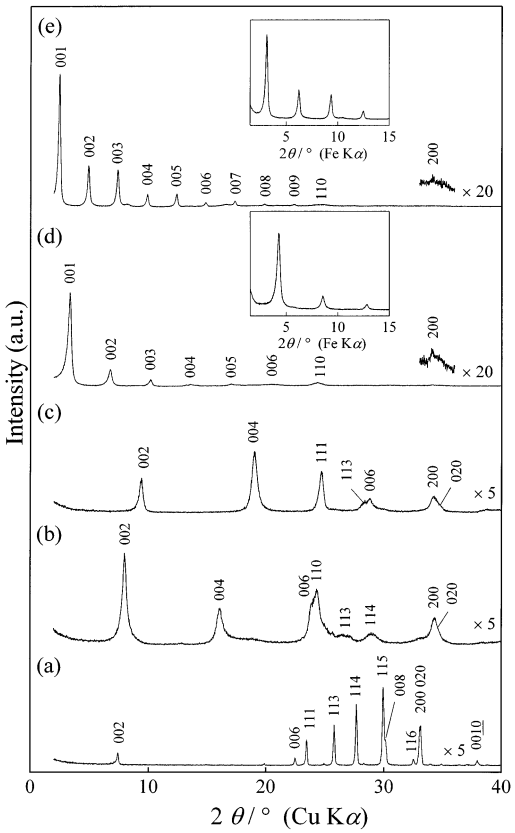

Figure 1. XRD patterns of (a) $Bi_2W_2O_9$, (b) air-dried acid-treated $Bi_2W_2O_9$, and (c) acid-treated $Bi_2W_2O_9$ dried at 120 °C, (d) (b) treated with the *n*-octylamine-heptane 1:1 mixture, and (e) (b) treated with the 1:1 *n*-dodecylamine−heptane mixture.

$Bi_2W_2O_9$ in 2.0 L of 6 M HCl), and 20 mL of a supernatant liquid were collected after 0.5, 1, 3, 6, 12, 24, and 72 h.

Intercalation of *n*-Alkylamines into the Acid-Treated $Bi_2W_2O_9$. About 2 g of air-dried acid-treated $Bi_2W_2O_9$ were reacted with 20 mL of *n*-octylamine (C8A)−heptane or *n*-dodecylamine (C12A)−heptane 1:1 mixture (as volume) at ambient temperature for 7 days. The product was separated by centrifugation, washed with heptane, and air-dried.

Analyses. XRD patterns were obtained with a Rigaku RINT-2500 diffractometer (monochromated Cu Kα radiation) or a MacScience $M0^3XHF^{22}$ diffractometer (Mn-filtered Fe Kα radiation). The amounts of metals were determined by ICP analysis (Nippon Jarrell Ash, ICAP575 MarkII). The samples were dissolved by heating in a mixture of HCl (5 mL), HNO_3 (5 mL), and HF (5 mL) at 200 °C for 2 h. A thermogravimetry (TG) curve of the acid-treated product was obtained on a thermobalance (MacScience, TG-DTA2000S, 10 °C/min). HREM images and electron diffraction (ED) patterns were obtained using a transmission electron microscope (JEOL JEM-4000EX) operated at 400 kV. The morphology was studied with scanning electron microscopy (SEM, Hitachi S-2500).

Results and Discussion

Acid-Treatment Process of $Bi_2W_2O_9$. Figure 1 demonstrates the XRD patterns of $Bi_2W_2O_9$ and its acid-treated products. $Bi_2W_2O_9$, which consists of bismuth oxide sheets and double-octahedral ReO_3-like slabs, shows intense (00*l*) reflections,[30] which are characteristic of layered structures. The *c* parameter [2.37063(5) nm] is doubled, because two successive ReO_3-type slabs show the relative displacement by $(a + b)/2$. Thus, the *c* parameter corresponds to the thickness of two bismuth oxide sheets and two ReO_3-like slabs.[31]

In the XRD pattern of the acid-treated product after air-drying (Figure 1b), all the reflections can be indexed on the basis of an orthorhombic cell. Upon acid treatment, the (00*l*) reflections of $Bi_2W_2O_9$ disappear and new (00*l*) reflections appear at higher angles, suggesting the formation of a layered structure with a smaller repeating distance through acid treatment. Corresponding to these shifts in the (00*l*) reflections, the *c* parameter of $Bi_2W_2O_9$ [2.37063(5) nm] decreases to 2.21(1) nm in the air-dried product. The (200) and (020) reflections of $Bi_2W_2O_9$ ($2\theta \approx 33.1°$)[30] should be observed in the same positions if no structural change in the ReO_3-like slabs occurs during acid treatment. In the XRD pattern of the air-dried product, however, no corresponding reflection is observed at $2\theta \approx 33.1°$, and reflections assignable to (200) and (020) are present at $2\theta = 34.2$ and 35.0°, respectively. Thus, the structure of the ReO_3-like slabs in $Bi_2W_2O_9$ is modified through acid treatment. The *a* and *b* parameters correspondingly decrease from those of $Bi_2W_2O_9$ [$a = 0.54377(1)$ nm and $b = 0.54166(1)$ nm] to $a = 0.524(1)$ nm and $b = 0.513(1)$ nm in the air-dried product.

The effect of drying on the air-dried product was also studied. When the variations in an XRD pattern profile upon drying at 50 °C were investigated, it was found that the (00*l*) reflections gradually shifted to higher angles. When the air-dried product was dried at 120 °C, the observed XRD pattern (Figure 1c) was identical to that of the product dried at 50 °C overnight. Thus, we analyzed the XRD pattern of the product dried at 120 °C further and indexed all the reflections on the basis of an orthorhombic cell. This analysis showed that the *c* parameter decreases with respect to that of the air-dried product [2.21(1) nm] to 1.86(1) nm in the product dried at 120 °C. The *a* and *b* parameters of the product dried at 120 °C are $a = 0.5249(2)$ nm and $b = 0.513(2)$ nm, which are closely similar to those of the air-dried product [$a = 0.524(1)$ nm and $b = 0.513(1)$ nm]. The reported lattice parameters for $H_2W_2O_7$ [$a = 0.5441(2)$ nm, $b = 0.5415(2)$ nm, and $c = 1.881(1)$ nm][29] do not show complete consistency with the observed values of the air-dried product and the product dried at 120 °C.

The suggestion of a layered structure for the acid-treated product is further supported by its intercalation behavior (Figure 1d,e). Upon treatment with *n*-alkylamines (C8A, C12A), the interlayer distances calculated from the (00*l*) reflections increase to 2.597(9) nm (C8A) and 3.56(2) nm (C12A). The (110) reflection (at 24.3°) and the (200) reflection, on the contrary, are present at the same 2θ angles after the intercalation reactions. These results indicate an expansion along the *c* axis with no structural change along the *a* and *b* axes and provide additional clear evidence for a layered structure of the acid-treated product. The mechanism appears to be an acid−base reaction of the type which is involved in the intercalation of organic bases into various protonated forms of layered oxides.[17,32] The exchange of protons with tetramethylammonium ions in the exfoliation

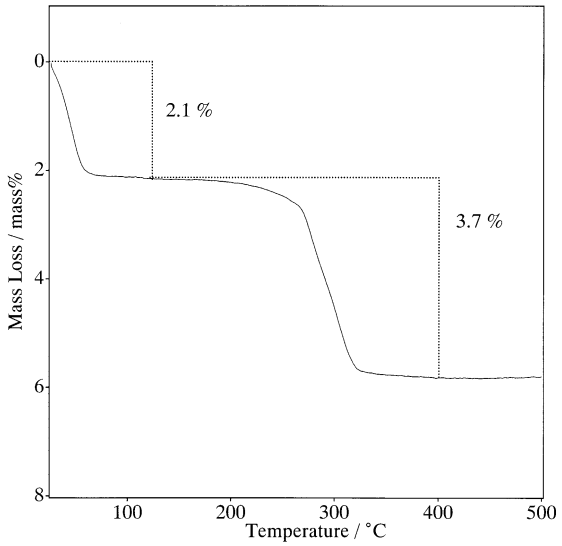

Figure 2. TG curve of air-dried acid-treated $Bi_2W_2O_9$.

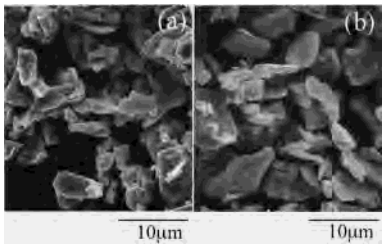

Figure 3. Scanning electron micrographs of (a) $Bi_2W_2O_9$ and (b) acid-treated $Bi_2W_2O_9$.

process of $H_2W_2O_7$[29] should also involve an intercalation process in the initial stage.

The composition of the acid-treated product is estimated on the basis of ICP and TG results. The Bi:W molar ratio in the acid-treated product was 0.01, indicating that essentially all of bismuth was leached by acid treatment. The TG curve of the air-dried product is shown in Figure 2. The mass loss ($\leq$400 °C) is clearly divided into two parts with an intermediate plateau. The first mass loss ($\leq$120 °C) can be ascribed to the loss of interlayer water, since the *c* parameter decreases without a collapse of the layers upon drying at 120 °C (Figure 1). The second mass loss (>180 °C) can then be ascribed to dehydration of the layers in the acid-treated product. With the second mass loss assigned to water and the remaining mass to WO_3, the WO_3:H_2O molar ratio is calculated as 2.0. Taking the first mass loss into account, we conclude that the compositions of the air-dried product is $H_2W_2O_7 \cdot nH_2O$ with a typical *n* value of 0.58 and that the product dried at 120 °C is $H_2W_2O_7$ (with $n = 0$).

The conversion could proceed either through dissolution of $Bi_2W_2O_9$ and subsequent crystallization of tungstic acid or through selective leaching of the bismuth oxide sheets in $Bi_2W_2O_9$ without dissolution. Thus, the change in morphology during acid treatment should provide critical information concerning the reaction mechanism (SEM; Figure 3). Both $Bi_2W_2O_9$ and its acid-treated product possess very similar platelike morphologies, and no notable change in particle size is observed. The concentrations of tungsten in the supernatant liquids (determined by ICP during the large-scale synthesis) were, moreover, always less than 1% of tungsten originally contained in $Bi_2W_2O_9$. These results clearly indicate that the present conversion reaction does not proceed through a dissolution−crystallization mechanism: a selective leaching process is highly likely.

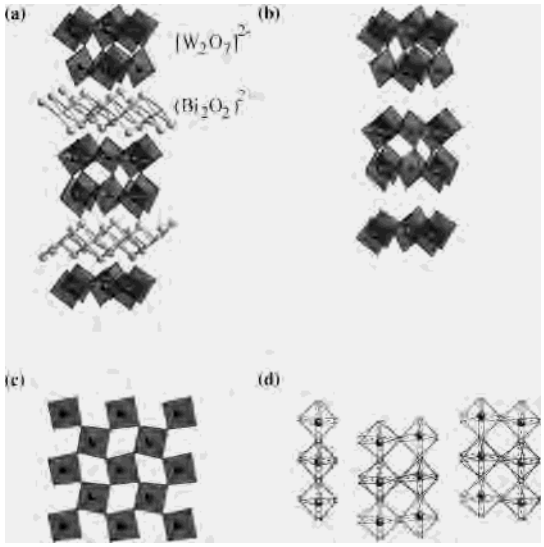

Figure 4. (a) Structure of $Bi_2W_2O_9$ and (b−d) proposed structural model of acid-treated $Bi_2W_2O_9$ ($H_2W_2O_7$): (b) overview; (c) [001] view; (d) [110] view.

Structural Characterization of the Acid-Treated Product, $H_2W_2O_7 \cdot nH_2O$. All the characterization results presented above suggest that bismuth oxide sheets are selectively leached and that protons ($2\ H^+/[W_2O_7]^{2-}$) and water molecules are introduced to form a new layered compound, $H_2W_2O_7 \cdot nH_2O$, which shows essential consistency with the previous report for $H_2W_2O_7$ formation.[29] The XRD results also clearly indicate that a slight structural change in the ReO_3-like slabs in $Bi_2W_2O_9$ occurs upon acid treatment, although SEM observation suggests selective leaching of the bismuth oxide sheets as a reaction mechanism. To demonstrate that the structure of $H_2W_2O_7 \cdot nH_2O$ can be reasonably derived from that of $Bi_2W_2O_9$, a preliminary structural model of $H_2W_2O_7$ is proposed. Since the changes in the *a* and *b* parameters are relatively small (96% along the *a* axis and 95% along the *b* axis), only a limited structural modification of the ReO_3-like slabs in $Bi_2W_2O_9$ appears necessary to simulate the structures of the layers in $H_2W_2O_7$. As a consequence, a preliminary structural model is derived from the reported structure of $Bi_2W_2O_9$[31] through removal of the bismuth oxide sheets from the structure of $Bi_2W_2O_9$, and thus, the space group of $Bi_2W_2O_9$ ($Pna2_1$)[31] is applied to the proposed model. The positions of the protons are not determined in the proposed model. The lattice parameters of the acid-treated product dried at 120 °C (corresponding to $H_2W_2O_7$) are employed for the proposed model. The arrangement of atoms in the *ab* plane is therefore essentially unchanged through this modification. The resultant structural model is shown in Figure 4b along with the structure of $Bi_2W_2O_9$ (Figure 4a). On the basis of this proposed prelimi-

(32) Lagaly, G. *Solid State Ionics* **1986**, *22*, 43−51.

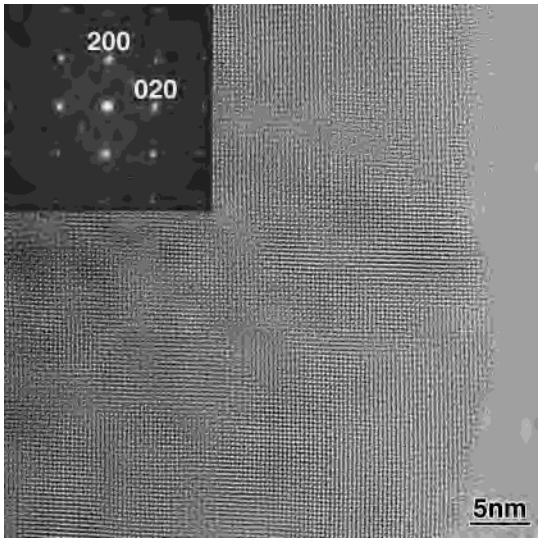

Figure 5. HREM image of acid-treated $Bi_2W_2O_9$ along [001]. A corresponding ED pattern is shown in the inset.

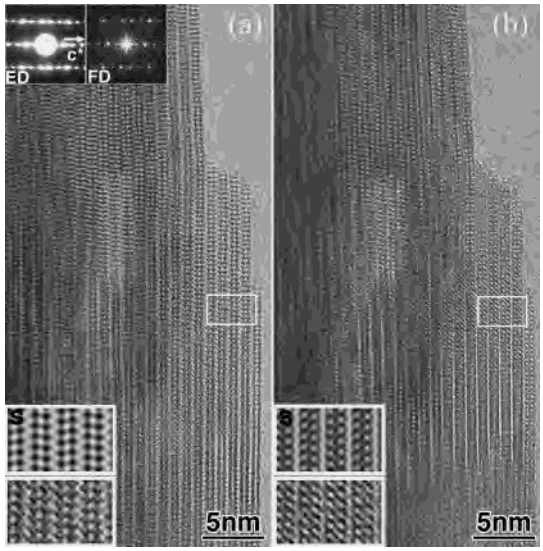

Figure 6. HREM images of acid-treated $Bi_2W_2O_9$ along [110]: (a) image recorded at a value close to Scherzer's defocus; (b) image recorded with an overfocus aberration. An enlarged image and corresponding simulated image are also shown in the insets for both HREM images. Corresponding Fourier diffractogram (FD) and ED are shown in the insets in the image (a). FD was obtained from a thin region including the area enclosed with a white rectangle.

nary model, we shall proceed to interpret the HREM images of $H_2W_2O_7 \cdot nH_2O$. It should be noted that the HREM images should correspond to $H_2W_2O_7$, since interlayer water molecules are removed during HREM observation conducted under vacuum.

The ED pattern of $H_2W_2O_7$ along the [001] zone axis and the corresponding HREM image are shown in Figure 5. The ED pattern corresponds to the *ab* plane of the orthorhombic cell, which is consistent with the indexing of the XRD pattern. The HREM image shows a regular dot array, which exhibits excellent consistency with the arrangement of tungsten atoms in the *ab* plane in the proposed model (Figure 4c).

The HREM image of $H_2W_2O_7$ along the [110] zone axis is shown in Figure 6. The HREM image was recorded at a value close to Scherzer's defocus, and the black dots therefore correspond to the tungsten atoms in Figure 6a. A layered structure with two sheets of tungsten atoms present in one layer is clearly revealed. A simulated image is calculated to verify the proposed model. An enlarged image and a corresponding simulated [110] image are demonstrated in the insets. A clear similarity is evident between these two images, indicating that the layers consist of two WO_6 octahedral sheets in a manner similar to the ReO_3-like slabs in $Bi_2W_2O_9$. In the ED pattern, diffusing streaks are clearly observed, and are ascribed to the presence of stacking faults (as shown by the HREM image). To analyze the structure, we performed Fourier transformation of the HREM image in a thin perfect region. The resulting Fourier diffractogram (FD) is also shown in the inset, and is consistent with the orthorhombic cell.

Figure 6b exhibits the HREM image recorded with overfocus aberration along the [110] zone axis. It should be noted that tungsten atoms are present as white dots in Figure 6b. An enlarged image and a corresponding simulated [110] image, shown as insets, exhibit excellent similarity, especially for the arrangement of W atoms, a result further supporting the validity of the proposed model (Figure 4d). The arrangement of the proposed model suggests that the *c* axis should be doubled, which is consistent with the observed *c* parameter of $H_2W_2O_7$ [1.86(1) nm]. This interpretation is supported by the observed repeating distance in the HREM image ($\sim$0.9 nm), which is in excellent agreement with *c*/2 (0.93 nm).

These HREM observations and simulated images based on the proposed model suggest that the structure of the double-octahedral layers in $H_2W_2O_7$ resembles that of the ReO_3-like slabs in the original $Bi_2W_2O_9$. Closer inspection of the observed [110] images and the proposed model, however, reveals a deviation of the actual structure of $H_2W_2O_7$ from the proposed model. To demonstrate this deviation, the angle between the (001) plane and the tie line connecting two dots (corresponding approximately to the tungsten atom positions) in the same layer (projected on the [110] direction) is employed. The angle in the simulated image based on the proposed preliminary model is $97 \pm 1°$, while that in the observed image is $91 \pm 2°$. This discrepancy could be ascribed to tungsten atom displacement, which is frequently observed in phase transition of WO_3,[33,34] but the variations in the *a* and *b* parameters upon acid treatment cannot be explained only by this displacement. In the structure of $Bi_2W_2O_9$, one apical oxygen in the WO_6 octahedron is weakly bound to bismuth atoms in the bismuth oxide sheet.[31] It is therefore reasonable to assume that the oxygen arrangement is also affected by selective leaching of the bismuth oxide sheets by acid treatment, leading to the shrinkage along the *a* and *b* axes. This change in oxygen arrangement can also be regarded as a change in the WO_6 octahedra arrangement. The WO_6 octahedra arrangement in $Bi_2W_2O_9$ is reported to be distorted, and the distortion is

(33) Woodward, P. M.; Sleight, A. W.; Vogt, T. *J. Phys. Chem. Solids* **1995**, *56*, 1305−1315.
(34) Woodward, P. M.; Sleight, A. W.; Vogt, T. *J. Solid State Chem.* **1997**, *131*, 9−17.

partly ascribed to the attraction of apical oxygen by bismuth atoms.[31] It appears, therefore, that the observed change in oxygen arrangement can be regarded as relaxation of the WO_6 octahedra arrangement upon the removal of the bismuth oxide sheets.

When the structures of $H_2W_2O_7{\cdot}nH_2O$ and $H_2W_2O_7$ are compared with that of $WO_3{\cdot}H_2O$, a single-octahedral layered compound with an orthorhombic cell, the *a* and *b* parameters of $H_2W_2O_7{\cdot}nH_2O$ and $H_2W_2O_7$ ($a = \sim 0.525$ nm and $b = \sim 0.513$ nm) are found to be closely similar to the corresponding lattice parameters of $WO_3{\cdot}H_2O$ ($a = 0.5249$ nm and $c = 0.5133$ nm; the *b* axis is perpendicular to the layers in a $WO_3{\cdot}H_2O$ structure).[6] These similarities strongly suggest that these three compounds possess a similar arrangement of the WO_6 octahedra: the observed *a* and *b* parameters of $H_2W_2O_7{\cdot}nH_2O$ and $H_2W_2O_7$ are reasonable for two-dimensionally linked WO_6 octahedra.

This conversion is unique among similar conversions,[17,21−24] because of the structural modification of the ReO_3-like slabs involved. The distortion of the WO_6 octahedra arrangement in $Bi_2W_2O_9$ is larger than that of other Aurivillius phases with a $Bi_2A_{n-1}B_nO_{3n+3}$ composition, indicating that the A-site cations regularize the perovskite-like slab structures.[31] The flexibility of the WO_6 octahedra network therefore also appears to be caused by the lack of A-site cations and to allow the structural change upon selective leaching of the bismuth oxide sheets. It should be noted that the WO_6 octahedra arrangement remains distorted even after the selective leaching of the bismuth oxide sheets. This appears to be ascribable to the cooperative antiparallel displacement of tungsten atoms, as observed in $Bi_2W_2O_9$,[31] Bi_2WO_6,[35] and WO_3.[34]

To examine the structure of $H_2W_2O_7{\cdot}nH_2O$ further, a one-dimensional electron density map projected on the *c* axis was calculated using five (00*l*) reflections of $H_2W_2O_7$ (dried at 120 °C). A one-dimensional electron density map was also calculated from the proposed model. These two profiles, shown in Figure 7, match with only a small discrepancy in intensity, a result adding strong support for the proposed structure of $H_2W_2O_7$. Two intense peaks are assignable as a contribution of tungsten atoms, and the W−W distance along the *c* axis is therefore estimated to be 0.39 nm. Since the W−W tie line deviates from the *c* axis only slightly, the distance along the *c* axis (0.39 nm) should be close to the actual W−W distance. The reported W−W distances in $Bi_2W_2O_9$,[31] $WO_3{\cdot}H_2O$,[6] and monoclinic and triclinic WO_3[33,34] are in the range of 0.365−0.392 nm and, thus, show reasonable consistency with the value observed in this study.

Conclusions

We have reported the conversion process of $Bi_2W_2O_9$ into a tungstic acid, $H_2W_2O_7{\cdot}nH_2O$, with a double-octahedral layered structure as well as its full characterization. The air-dried product is $H_2W_2O_7{\cdot}nH_2O$ (typically $n = 0.58$) with interlayer water [$a = 0.524(1)$ nm, $b = 0.513(1)$ nm, and $c = 2.21(1)$ nm]. The product dried at 120 °C is $H_2W_2O_7$ with similar *a* and *b* parameters and a smaller *c* parameter [$a = 0.5249(2)$ nm, $b = 0.513(2)$ nm, and $c = 1.86(1)$ nm]. The proposal of a layered structure is strongly supported by successful intercalation of *n*-alkylamines (*n*-octylamine and *n*-dodecylamine). No evidence for the dissolution−recrystallization mechanism was provided by SEM observations, a result suggesting selective leaching of bismuth oxide sheets as a reaction mechanism. The HREM observations clearly indicate that the arrangement of tungsten atoms in the double-octahedral layers in $H_2W_2O_7{\cdot}nH_2O$ is similar to those in the ReO_3-like slabs in original $Bi_2W_2O_9$. Closer inspection of the [110] image, moreover, indicates a change in the WO_6 octahedra arrangement. Since one apical oxygen in each WO_6 octahedron is attracted by bismuth atoms in $Bi_2W_2O_9$ [$a = 0.54377(1)$ nm and $b = 0.54166(1)$ nm], the slight decrease in the *a* and *b* parameters upon acid treatment appears to be ascribable to a change in the WO_6 octahedra arrangement through the selective leaching of bismuth oxide sheets. Thus, all the results presented clearly show that this conversion proceeds through a "*chimie douce*"-type process involving selective leaching of bismuth oxide sheets. Besides the uniqueness of the conversion process, resultant $H_2W_2O_7{\cdot}nH_2O$ could be interesting because of its possible properties originating from a double-octahedral layered structure.

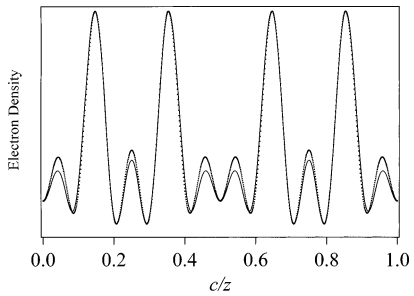

Figure 7. One-dimensional electron density maps projected on the *c* axis. The solid line is from experimental data for acid-treated $Bi_2W_2O_9$ (dried at 120 °C), and the dotted line is from the proposed model.

Acknowledgment. The authors gratefully thank Prof. Kazuyuki Kuroda, Department of Applied Chemistry at Waseda University, for his valuable discussions and Ms. Fumi Nakasone for her assistance. This work was financially supported in part by the Grant-in-Aid for Scientific Research (No. 14350462) from the Ministry of Education, Science, Sports, and Culture of Japan.

IC0206746

(35) Knight, K. S. *Mineral. Mag.* **1992**, *56*, 399−409.